

Dynamic disorder in methylammoniumtrihalogenoplumbates (II) observed by millimeterwave spectroscopy

A. Poglitsch and D. Weber

Citation: *J. Chem. Phys.* **87**, 6373 (1987); doi: 10.1063/1.453467

View online: <http://dx.doi.org/10.1063/1.453467>

View Table of Contents: <http://jcp.aip.org/resource/1/JCPSA6/v87/i11>

Published by the [American Institute of Physics](http://www.aip.org/).

Additional information on *J. Chem. Phys.*

Journal Homepage: <http://jcp.aip.org/>

Journal Information: http://jcp.aip.org/about/about_the_journal

Top downloads: http://jcp.aip.org/features/most_downloaded

Information for Authors: <http://jcp.aip.org/authors>

ADVERTISEMENT

physicstoday

Comment on any
Physics Today article.

Measured energy in Japan
David von Seggern
(vonseg@seismo.unr.edu) University of Nevada
July 2012, page 10
DIGITAL OBJECT IDENTIFIER
<http://dx.doi.org/10.1063/PT.3.1619>
The article by Thorne Lay and Hiroo Kanamori is an excellent review of the relationship between seismic moment and energy release. The authors note that the seismic moment is a measure of the size of the rupture, while that of a 100-megaton explosion is approximately five times as much energy as that of a 100-megaton nuclear detonation event—a 40-megaton atmospheric event is approximately five times as much energy by a factor of about 3, or 15 times as much energy as that of a 100-megaton nuclear device. I believe the authors used the relation for seismic energy release rather than total strain energy release. The seismic energy underestimates the total strain energy release by a variable that depends on friction on the fault plane. Accounting for total strain energy release would increase the earthquake energy number by orders of magnitude. Despite the catastrophic damage potential of nuclear bombs, the forces of nature occasionally unleash much larger energy releases. Although the nuclear bombs are under our control, earthquakes, volcanic eruptions, and extreme weather events are not. However, by judicious preparation and avoidance measures, humans can significantly diminish the damage of natural events.

Comment on this article
By the act of hitting a ball with a bat, one calculates the force energy to deliver the ball to its new location, but one must also take into account that the ball extended its energy release to that which became struck by the ball as its momentum ceased and passed energy to the struck team. Therefore the parameters of the damage extend into the future when the received energy to that pushed upon, later becomes released in a new event. Perhaps calculations of one added that in while another's calculations did not. E.M.C.
Written by Edgar Mocarvill, 14 July 2012 19:59

Dynamic disorder in methylammoniumtrihalogenoplumbates (II) observed by millimeter-wave spectroscopy

A. Poglitsch^{a)} and D. Weber

Max-Planck-Institut für Festkörperforschung, Postfach 80 06 65 7000 Stuttgart 80, Federal Republic of Germany

(Received 26 January 1987; accepted 14 August 1987)

The temperature-dependent structure of crystalline methylammoniumtrihalogenoplumbates (II)— $\text{CH}_3\text{NH}_3^+\text{PbX}_3^-$ ($X = \text{Cl, Br, I}$)—as determined by x-ray diffraction, is compared with measurements of the temperature-dependent complex permittivity at frequencies of 50–150 GHz. The dielectric measurements reveal a picosecond relaxation process which corresponds to a dynamic disorder of the methylammonium group in the high-temperature phases of the trihalogenoplumbates.

INTRODUCTION

As compounds crystallizing with the perovskite type structure,^{1,2} $\text{CH}_3\text{NH}_3^+\text{PbX}_3^-$ ($X = \text{Cl, Br, I}$) show a special feature: the CH_3NH_3^+ cation cannot be fixed in the crystal structure determination. This can be caused either by a disordered orientation or by a mobility of the cation in the crystal. Attempts at contactless conductivity measurement³ showed high absorption at 10 GHz, which, however, does not allow one to distinguish uniquely between conductivity and other dissipative processes. An investigation of the complex permittivity over an extended frequency and temperature range, therefore, was required.

SYNTHESIS

Methylammoniumtrihalogenoplumbate (II)— $\text{CH}_3\text{NH}_3^+\text{PbX}_3^-$ ($X = \text{Cl, Br, I}$)—was synthesized in concentrated aqueous solution of the acid HX which contained Pb^{2+} ions [from lead (II) acetate] and a respective amount of CH_3NH_3^+ (by adding a 40% solution of CH_3NH_2 in water). Beautiful crystals are grown by cooling an aqueous solution from about 100 °C to room temperature. However, in the case of $\text{CH}_3\text{NH}_3^+\text{PbI}_3^-$, the temperature must not be lowered below 40 °C because there the formation of colorless crystals of $\text{CH}_3\text{NH}_3^+\text{PbI}_3^- \cdot \text{H}_2\text{O}$ begins. Color of the perovskite type phases: $X = \text{Cl}$: colorless; $X = \text{Br}$: orange; $X = \text{I}$: black.

STRUCTURE ANALYSIS OF $\text{CH}_3\text{NH}_3^+\text{PbX}_3^-$

The temperature-dependent crystal structure of compounds $\text{CH}_3\text{NH}_3^+\text{PbX}_3^-$ was deduced from temperature-dependent Guinier–Simon photographs of the powdered crystals. The results of these measurements are summarized in Table I.

A single crystal structure determination was performed from $\text{CH}_3\text{NH}_3^+\text{PbBr}_3^-$ and $\text{CH}_3\text{NH}_3^+\text{PbI}_3^-$ at room temperature. The cubic perovskite structure of $\text{CH}_3\text{NH}_3^+\text{PbBr}_3^-$ (space group $Pm\bar{3}m$) (Fig. 4) is dominated by high temperature factors U_{22} and U_{33} ($= 1360 \text{ pm}^2$) of the Br ions perpendicular to the Pb–Br direction. A sec-

ond important result is the fact that the position of the CH_3NH_3^+ cation cannot be fixed due to the cubic symmetry which, for example, requires eight identical positions with the coordinates x, x, x for the cation in such a way that the tetrahedral coordinated C and N atoms show random distribution inside the eight tetrahedra of the cuboctahedra around the normal A position ($1/2, 1/2, 1/2$) of the perovskite ABX_3 .

$\text{CH}_3\text{NH}_3^+\text{PbI}_3^-$ forms a tetragonal structure at room temperature (space group $I4/m$ or $I4/mcm$). The transition to the cubic phase ($T_c = 327.4 \text{ K}$) is accompanied by a slight distortion of the PbI_6 octahedra around the c axes. The CH_3NH_3^+ cation cannot be fixed there, either. Its position might be an eightfold disordered one.

In all cases lowering the temperature of the cubic phases causes the transition to a phase with tetragonal symmetry. This first transition preserves the disordered character of the CH_3NH_3^+ cation. Finally the transition from the tetragonal symmetry to an orthorhombic symmetry reduces the disordering of CH_3NH_3^+ occupation. The cation gets a fixed position in the orthorhombic phase of $\text{CH}_3\text{NH}_3^+\text{PbBr}_3^-$ and $\text{CH}_3\text{NH}_3^+\text{PbI}_3^-$ (space group $Pna2_1$) whereas the orthorhombic phase of $\text{CH}_3\text{NH}_3^+\text{PbCl}_3^-$ ($P222_1$) now offers a twofold disordered position for the CH_3NH_3^+ cation. The transition from tetragonal to orthorhombic symmetry reveals an important fact because in all cases there is a transition from centrosymmetric to an acentric unit cell which is able to create ferroelectric or antiferroelectric phenomena. Therefore, further examination of these systems is in progress.

Temperature-dependent vibration spectra in the FIR region¹² from the colorless perovskite $\text{CH}_3\text{NH}_3^+\text{PbCl}_3^-$ are in agreement with these data. There is no fine structure above 200 K in the cubic phase. But at 150 K—the region of the orthorhombic phase—we get a spectrum with sharp vibration lines induced by the regular motion of the atomic groups according to the space group.

DYNAMICS

The question remains whether a static disorder or a dynamic process is responsible for the missing x-ray diffraction pattern of the CH_3NH_3^+ group in the high temperature

^{a)} Present address: Max-Planck-Institut für Extraterrestrische Physik, D-8046 Garching, FRG.

TABLE I. Temperature dependent structural data of $\text{CH}_3\text{NH}_3^+ \text{PbX}_3^-$ ($X = \text{Cl}, \text{Br}, \text{I}$).

Phase	Temperature (K)	Crystal system	Space group	Lattice (pm)	Volume (10^6 pm^3)
$\text{CH}_3\text{NH}_3^+ \text{PbCl}_3^-$					
α	> 178.8	cubic	$P m\bar{3}m$	$a = 567.5$	182.8
β	172.9–178.8	tetragonal	$P 4/mmm$	$a = 565.6$ $c = 563.0$	180.1
γ	< 172.9	orthorhombic	$P 222_1$	$a = 567.3$ $b = 562.8$ $c = 1118.2$	357.0
$\text{CH}_3\text{NH}_3^+ \text{PbBr}_3^-$					
α	> 236.9	cubic	$P m\bar{3}m$	$a = 590.1(1)$	206.3 (260 K)
β	155.1–236.9	tetragonal	$I 4/mcm$	$a = 832.2(2)$ $c = 1183.2(7)$	819.4
γ	149.5–155.1	tetragonal	$P 4/mmm$	$a = 589.4(2)$ $c = 586.1(2)$	
δ	< 144.5	orthorhombic	$P na2_1$	$a = 797.9(1)$ $b = 858.0(2)$ $c = 1184.9(2)$	811.1
$\text{CH}_3\text{NH}_3^+ \text{PbI}_3^-$					
α	> 327.4	cubic	$P m\bar{3}m$	$a = 632.85(4)$	253.5
β	162.2–327.4	tetragonal	$I 4/mcm$	$a = 885.5(6)$ $c = 1265.9(8)$	992.6
γ	< 162.2	orthorhombic	$P na2_1$	$a = 886.1(2)$ $b = 858.1(2)$ $c = 1262.0(3)$	959.5

phases. The CH_3NH_3^+ ion has a permanent electric dipole moment; thus a dynamic process changing the orientation of this ion can contribute to the dielectric properties of the substances. We therefore investigated the frequency and temperature dependence of the complex permittivity at millimeter-wave frequencies.

EXPERIMENTAL

The measurements were carried out with a dispersive polarizing millimeter-wave interferometer⁴ at frequencies between 50 and 150 GHz. This instrument allows the determination of both the real part ϵ' and the imaginary part ϵ'' of the dielectric constant by measuring the amplitude attenuation and the phase shift of the millimeter wave when passing through the sample. The samples were plane parallel disks of 48 mm diameter and of about 1 mm thickness. They were prepared by pressing the powderized materials in a polished stainless-steel mold at a pressure of 25 kN/cm². For low-temperature measurements between 100 and 300 K, a closed styrofoam box was used. Styrofoam provides both sufficient thermal insulation and high transparency for millimeter waves. The sample temperature was set by a temperature-controlled nitrogen gas flow through the box.

RESULTS

The complex permittivity of $\text{CH}_3\text{NH}_3^+ \text{PbCl}_3^-$, $\text{CH}_3\text{NH}_3^+ \text{PbBr}_3^-$, and $\text{CH}_3\text{NH}_3^+ \text{PbI}_3^-$ has been measured at 90 GHz between 100 and 300 K. Additionally, for $\text{CH}_3\text{NH}_3^+ \text{PbBr}_3^-$ measurements have been carried out at 50 and 150 GHz. The results are shown in Figs. 1, 2, and 3, respectively. A discontinuity in the dielectric constant occurs for all three substances at the phase transition from the orthorhombic phase to the tetragonal phase. Above the respective temperature, the real part ϵ' of the dielectric constant increases monotonically with temperature. A similar

behavior is found for the imaginary part ϵ'' except for the measurement on $\text{CH}_3\text{NH}_3^+ \text{PbBr}_3^-$ at 50 GHz where a maximum is observed at 260 K. Both parts of ϵ are approximately

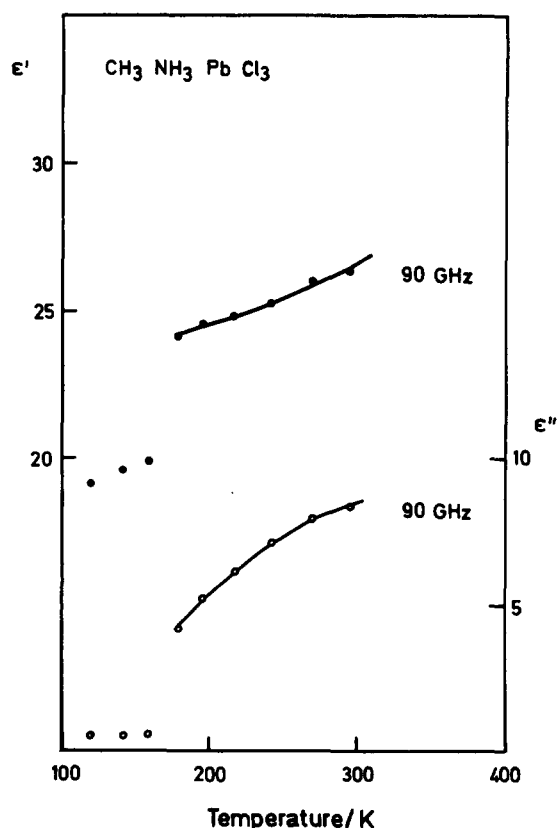


FIG. 1. The complex permittivity of $\text{CH}_3\text{NH}_3^+ \text{PbCl}_3^-$ from 100 to 300 K at frequency 90 GHz. Filled circles represent the real part ϵ' , open circles represent the imaginary part ϵ'' . Lines represent the model function [Eqs. (1) and (2) with fit parameters of Table I].

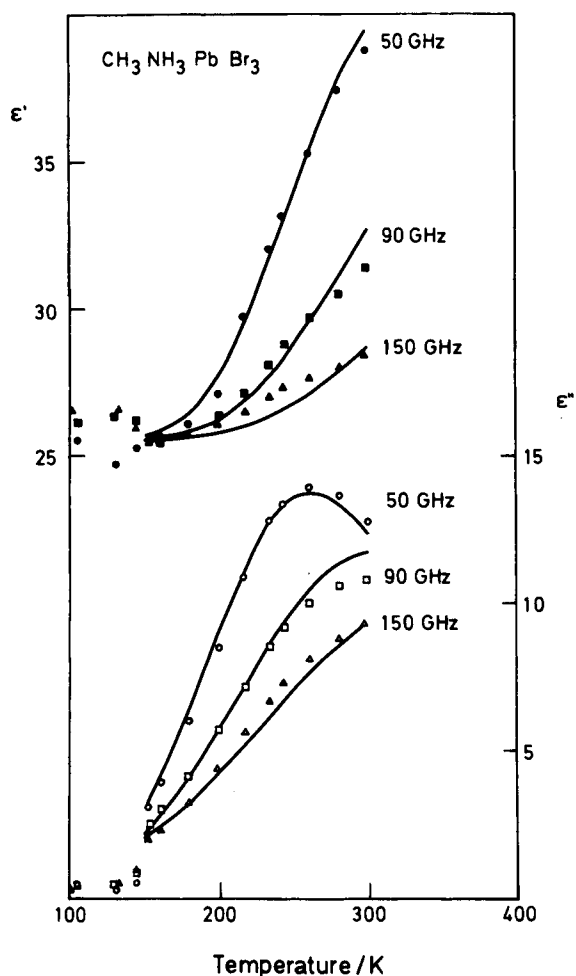


FIG. 2. The complex permittivity of $\text{CH}_3\text{NH}_3^+\text{PbBr}_3^-$ from 100 to 300 K at frequencies 50, 90, and 150 GHz. Filled symbols represent the real part ϵ' , open symbols represent the imaginary part ϵ'' . Lines represent the model function [Eqs. (1) and (2) with fit parameters of Table I].

inverse proportional to the frequency. The further phase transitions seem to have no significant influence on the dielectric constant of the materials, though there might be some change in the slope of the measurements on $\text{CH}_3\text{NH}_3^+\text{PbBr}_3^-$ at the phase transition from the tetragonal to the cubic phase. It should be noted that with $\text{CH}_3\text{NH}_3^+\text{PbBr}_3^-$ a new sample had to be prepared for each frequency because the samples showed fissures after a cooling-down/warming-up cycle. These may have introduced some systematic error.

DISCUSSION

To draw any conclusion on the microscopic level, it is necessary to check possible mechanisms underlying the observed temperature and frequency dependence of the complex permittivity.

The maximum of ϵ'' vs temperature in the 50 GHz measurement on $\text{CH}_3\text{NH}_3^+\text{PbBr}_3^-$ as well as the frequency dependence indicate a dipole relaxation.^{5,6}

We therefore tried to fit the data at temperatures above the phase transition with a Debye relaxation⁷

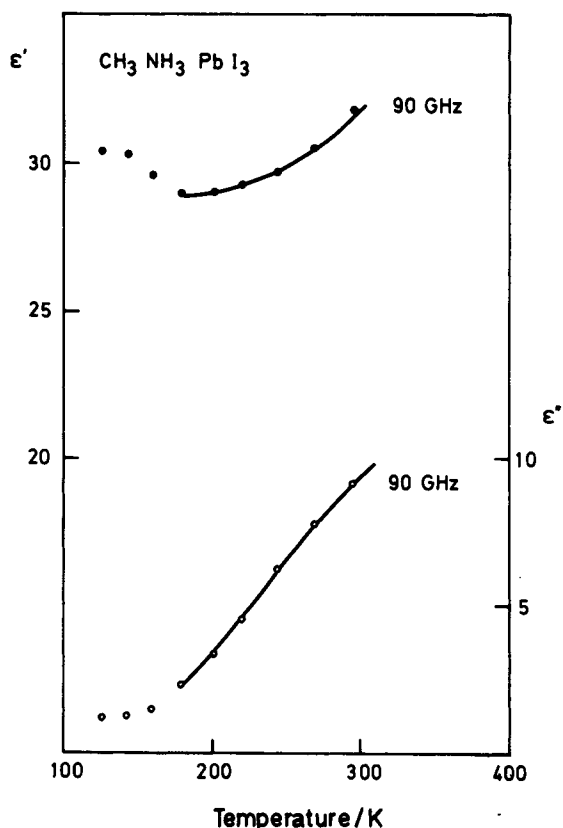


FIG. 3. The complex permittivity of $\text{CH}_3\text{NH}_3^+\text{PbI}_3^-$ from 100 to 300 K at frequency 90 GHz. Filled circles represent the real part ϵ' , open circles represent the imaginary part ϵ'' . Lines represent the model function [Eqs. (1) and (2) with fit parameters of Table I].

$$\tilde{\epsilon} = \epsilon_\infty + \frac{C}{T} \cdot \frac{1}{1 - i\omega\tau(T)}, \quad (1)$$

where the temperature dependence of the relaxation time τ is given by

$$\tau = \tau_\infty \cdot e^{A/T}. \quad (2)$$

The factor C/T determines the contribution of the relaxation to the static dielectric constant. The fit function is represented by solid lines in Figs. 1, 2, and 3. The parameters according to Eqs. (1) and (2) are shown in Table II. Additionally, the relaxation times at room temperature are given there.

In the case $\text{CH}_3\text{NH}_3^+\text{PbBr}_3^-$, a term $i\tilde{B}\omega$ had to be added to the dielectric function to obtain the observed frequency dependence at low temperatures. This term could correspond to disorder-induced single-phonon absorption, to the low-frequency wing of a far-infrared band, or to multiphonon difference processes. For the other substances, this (small) correction could not be determined because measurements have been done at one frequency only. Even in the case of $\text{CH}_3\text{NH}_3^+\text{PbBr}_3^-$ it does not seem reasonable to consider extensions of the Debye function like the Cole-Cole function^{6,8} because measurements have been carried out in a restricted frequency range only. The high-frequency dielectric constant ϵ_∞ shows a systematic increase as function of the mass of the halide ion. This can be due to the shift of the lattice-vibration modes to lower frequencies with increasing mass.

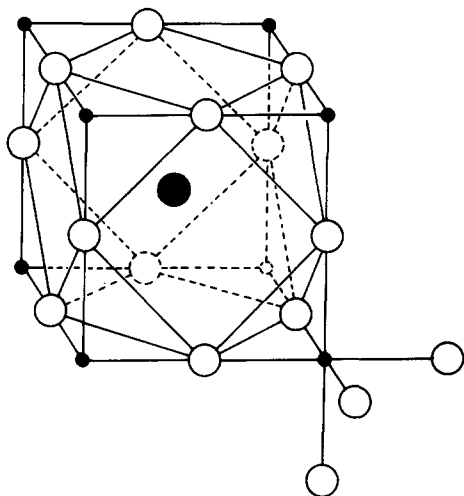


FIG. 4. Cubic perovskite structure ABX_3 ; A: dotted large circle; B: filled small circle; X: empty large circle. The cuboctahedral environment of A is marked, too.

The microscopic picture behind the phenomenological description of a relaxation process by the Debye function is the orientation of an ensemble of dipolar units in an applied electric field and the reestablishment of disorder by thermal fluctuations within the relaxation time τ when the field is switched off. For liquids and polymers, the temperature dependence of the relaxation time τ is derived from the temperature dependence of the viscosity—a quantity that does not apply well for a crystalline solid. In solids it is reasonable to assume several possible orientations of minimal energy for a dipolar unit separated by potential barriers.⁵ For the three substances investigated here, the coincidence between the onset of microwave absorption and the structural request of a highly disordered CH_3NH_3^+ ion shows that this dipolar unit undergoes the relaxation process. The cubic crystal symmetry suggests eight equivalent orientations of the CH_3NH_3^+ group along the body diagonals of a cube as shown in Fig. 5. This means each orientation has three adjacent orientations to and from which transitions over an assumed potential barrier A can be caused by thermal fluctuations. The rate r_{ij} for each of these elementary transitions between two neighboring transitions can be written as

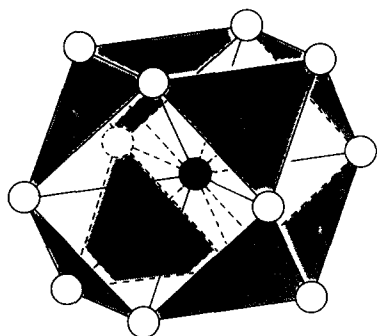


FIG. 5. Eight tetrahedra inside the cuboctahedra around the position $1/2, 1/2, 1/2$ ($= A$). The $\text{H}_3\text{C}-\text{NH}_3$ unit occupies two edge-shared tetrahedra; thus having eight possible orientations. Transitions are assumed to occur from and to the respective three next-neighbor positions.

TABLE II. Parameters used for fitting the data according to Eqs. (1) and (2) for the three substances $\text{CH}_3\text{NH}_3^+\text{PbX}_3^-$ ($X = \text{Cl}, \text{Br}, \text{I}$), and derived values for the microscopic dipole moment μ according to Eq. (6).

	$\text{CH}_3\text{NH}_3^+\text{PbCl}_3^-$	$\text{CH}_3\text{NH}_3^+\text{PbBr}_3^-$	$\text{CH}_3\text{NH}_3^+\text{PbI}_3^-$
ϵ_∞	23.9	25.5	28.8
$C(\text{K})$	8960	7274	9434
$U(\text{K})$	567.5	910	910
τ_∞	0.849	0.131	0.259
$\tau(300\text{K})(\text{ps})$	5.63	2.73	5.37
$B(\text{GHz}^{-1})$...	1.19×10^{-3}	...
$\bar{V}_{\text{uc}}(10^6 \text{pm}^3)$	182.8	206.3	253.5
η	8.63	9.17	10.27
$\mu(\text{C m})$	2.84×10^{-30}	2.56×10^{-30}	2.85×10^{-30}
$\mu(\text{D})$	0.85	0.766	0.854

$$r_{ij} = r_{ji} = r = r_\infty \cdot e^{-A/T}. \quad (3)$$

The rate equations for the occupation numbers of the eight different orientations lead to a homogeneous system of linear differential equations. As shown in the Appendix, only one solution with the eigenvalue $\lambda = 2r$ has a resulting dipole moment and can therefore be probed by an electric field; so a single relaxation process with relaxation time $\tau = 1/\lambda$ is predicted. This justifies within our model the description of the dielectric function by Eqs. (1) and (2). The fit parameter C is then referred to the microscopic dipole moment μ of the CH_3NH_3^+ group by

$$C = N\mu^2\eta/3k\epsilon_0, \quad (4)$$

where N is the volume density of dipoles, k is the Boltzmann constant, and ϵ_0 is the vacuum permittivity (SI). The dimensionless quantity η is the correction for the Lorentz local field which for cubic and tetragonal symmetry is given by

$$\eta = (\epsilon_\infty + 2)/3, \quad (5)$$

with ϵ_∞ being the high-frequency dielectric constant of the material. We rewrite Eq. (4) to obtain

$$\mu = (3Ck\epsilon_0\bar{V}_{\text{uc}}/\eta)^{1/2}, \quad (6)$$

where \bar{V}_{uc} is the volume of the crystal's unit cell divided by the number of CH_3NH_3^+ ions per unit cell. The derived values for μ are given in Table II. They confirm our assignment of the relaxation process to this group. It is, however, possible that the halide ions are affected by the fluctuations of the CH_3NH_3^+ group; this would also explain their unusually large thermal ellipsoids. Moreover, such coupling could be responsible for different potential barriers and relaxation times with different halide ions.

The relaxation times τ found for the three substances to be a few picoseconds at room temperature may appear rather short; on the other hand similar relaxation times have been observed in molecular crystals containing the polar peptide unit⁹ and in proteins and biopolymers.^{10,11} Moreover, these results together give rise to the assumption that rapid relaxations might be a rather general phenomenon in solids with molecular units and it seems worthwhile to study them both in structure and dynamics.

ACKNOWLEDGMENTS

We would like to thank Professor L. Genzel and Professor H. G. v. Schnering for helpful discussions. Thanks to Dr. W. Bauhofer for bringing us to each other's attention and to M. Haggerty for his critical reading of our manuscript.

APPENDIX

We want to give a short derivation of our relaxation model. As shown in Fig. 5 we assume eight possible orientations of the dipole. Transitions can take place to and from the three next-neighboring positions leading to a system of rate equations for the occupation numbers N_j :

$$\frac{dN_j}{dt} + 3rN_j - r \sum_{i=1}^3 N_{ji} = 0, \quad (\text{A1})$$

where j runs from 1 to 8, r is the transition rate, and the N_{ji} denote the occupation numbers of the three next neighbors of the orientation with index j . With the ansatz

$$N_j = n_j \cdot e^{-\lambda t}, \quad (\text{A2})$$

and the abbreviation

$$x = \lambda / r, \quad (\text{A3})$$

we get

$$n_j(3 - x) - \sum_{i=1}^3 n_{ji} = 0. \quad (\text{A4})$$

The eigenvalues of the coefficient matrix are found to be

$$x_1 = 0, \quad \lambda_1 = 0, \quad (\text{A5})$$

$$x_2 = 2, \quad \lambda_2 = 2r, \quad (\text{A6})$$

$$x_3 = 4, \quad \lambda_3 = 4r, \quad (\text{A7})$$

$$x_4 = 6, \quad \lambda_4 = 6r. \quad (\text{A8})$$

The solution to the first eigenvalue is given by

$$n_1 = n_2 = n_3 = n_5 = n_6 = n_7 = n_8 = 1/8. \quad (\text{A9})$$

This is the time-independent distribution without an external field. Any time-dependent solution will be a superposition on this solution.

The solution to the second eigenvalue is given by

$$n_1 = -n_8, \quad (\text{A10})$$

$$n_2 = -n_5, \quad (\text{A11})$$

$$n_3 = -n_6, \quad (\text{A12})$$

$$n_4 = -n_7, \quad (\text{A13})$$

$$n_1 + n_3 = n_2 + n_4; \quad n_5 + n_7 = n_6 + n_8. \quad (\text{A14})$$

The solution to the third eigenvalue is given by

$$n_1 = n_8, \quad (\text{A15})$$

$$n_2 = n_5, \quad (\text{A16})$$

$$n_3 = n_6, \quad (\text{A17})$$

$$n_4 = n_7, \quad (\text{A18})$$

$$n_1 + n_2 + n_3 + n_4 = 0. \quad (\text{A19})$$

The solution to the fourth eigenvalue is given by

$$\begin{aligned} n_1 = n_3 = n_5 = n_7 \\ = -n_2 = -n_4 = -n_6 = -n_8. \end{aligned} \quad (\text{A20})$$

It is easily seen from Fig. 4 that only the solution to the second eigenvalue $\lambda_2 = 2r$ has a resulting dipole moment and will, therefore, couple to an applied electric field. This also means that one will observe a single relaxation instead of an eventual superposition of several ones.

We now calculate the contribution of the dipoles to the polarization of the crystal. The dipole vectors in the eight orientations according to Fig. 4 are given by

$$\boldsymbol{\mu}_1 = \mu/3^{1/2} \cdot (1, -1, 1), \quad (\text{A21})$$

$$\boldsymbol{\mu}_2 = \mu/3^{1/2} \cdot (1, 1, 1), \quad (\text{A22})$$

$$\boldsymbol{\mu}_3 = \mu/3^{1/2} \cdot (-1, 1, 1), \quad (\text{A23})$$

$$\boldsymbol{\mu}_4 = \mu/3^{1/2} \cdot (-1, -1, 1), \quad (\text{A24})$$

$$\boldsymbol{\mu}_5 = \mu/3^{1/2} \cdot (-1, -1, -1), \quad (\text{A25})$$

$$\boldsymbol{\mu}_6 = \mu/3^{1/2} \cdot (1, -1, -1), \quad (\text{A26})$$

$$\boldsymbol{\mu}_7 = \mu/3^{1/2} \cdot (1, 1, -1), \quad (\text{A27})$$

$$\boldsymbol{\mu}_8 = \mu/3^{1/2} \cdot (-1, 1, -1), \quad (\text{A28})$$

with μ being the absolute value of the molecular dipole moment. Without an external field it follows from Eqs. (A9) and (A21)–(A28) for the statistical average of the dipole moment

$$\langle \boldsymbol{\mu} \rangle_0 = \sum_{i=1}^8 n_i \cdot \boldsymbol{\mu}_i = \frac{1}{8} \cdot \sum_{i=1}^8 \boldsymbol{\mu}_i = 0. \quad (\text{A29})$$

In a static electric field \mathbf{F} the occupation numbers n_{iF} will be determined by a Boltzmann distribution

$$n_{iF} = \frac{e^{\boldsymbol{\mu}_i \cdot \mathbf{F} / kT}}{\sum_{j=1}^8 e^{\boldsymbol{\mu}_j \cdot \mathbf{F} / kT}} \approx \frac{1 + \boldsymbol{\mu}_i \cdot \mathbf{F} / kT}{8 + (\sum_{j=1}^8 \boldsymbol{\mu}_j) \cdot \mathbf{F} / kT}, \quad (\text{A30})$$

with Eq. (A29) we can write Eq. (A30) as

$$n_{iF} = \frac{1}{8} + \frac{\boldsymbol{\mu}_i \cdot \mathbf{F} / kT}{8} = n_0 + \frac{\boldsymbol{\mu}_i \cdot \mathbf{F} / kT}{8}. \quad (\text{A31})$$

The mean value of the dipole moment will then be

$$\langle \boldsymbol{\mu} \rangle_F = \sum_{i=1}^8 n_{iF} \cdot \boldsymbol{\mu}_i = \frac{1}{8} \sum_{i=1}^8 \boldsymbol{\mu}_i + \frac{1}{8} \sum_{i=1}^8 \boldsymbol{\mu}_i \cdot \frac{(\boldsymbol{\mu}_i \cdot \mathbf{F})}{kT}. \quad (\text{A32})$$

Again by Eq. (A29) we get

$$\langle \boldsymbol{\mu} \rangle_F + \frac{1}{8} \sum_{i=1}^8 (\boldsymbol{\mu}_i \cdot \mathbf{F}) / kT = \frac{1}{8} \left(\sum_{i=1}^8 \boldsymbol{\mu}_i \cdot \boldsymbol{\mu}_i \right) \cdot \mathbf{F} / kT, \quad (\text{A33})$$

where $\boldsymbol{\mu}_i \cdot \boldsymbol{\mu}_i$ shall denote the dyadic product. From Eqs. (A21)–(A28) it follows that

$$\sum_{i=1}^8 \boldsymbol{\mu}_i \cdot \boldsymbol{\mu}_i = \frac{8}{3} \mu^2, \quad (\text{A34})$$

and we get

$$\langle \boldsymbol{\mu} \rangle_F = \frac{\mu^2}{3kT} \cdot \mathbf{F}. \quad (\text{A35})$$

The polarization is then given by

$$\mathbf{P} = N \cdot \langle \boldsymbol{\mu} \rangle_F = \frac{N\mu^2}{3kT} \cdot \mathbf{F}. \quad (\text{A36})$$

From the exponential time dependence in Eq. (A2), it follows for the polarization in a periodic field of angular frequency ω :

$$\mathbf{P}(\omega) = \frac{N\mu^2}{3kT} \cdot \frac{1}{1 - i\omega\tau} \cdot \mathbf{F}(\omega), \quad (\text{A37})$$

where the relaxation time τ is given by Eq. (A6):

$$\tau = 1/\lambda_2 = 1/2r. \quad (\text{A38})$$

Note that the field \mathbf{F} always is the local electric field which is determined both by the external field and the symmetry and the dielectric constant of the crystal.

¹D. Weber, Z. Naturforsch Teil B 33, 1443 (1978).

²D. Weber (to be published).

³W. Bauhofer, J. Phys. E 14, 934 (1981).

⁴L. Genzel, A. Poglitsch, and S. Häsel, Int. J. Infrared MM Waves 6, 741 (1985).

⁵H. Fröhlich, *Theory of Dielectrics* (Clarendon, Oxford, 1958).

⁶C. J. F. Böttcher and P. Bordewijk, *Theory of Electric Polarization* (Elsevier, Amsterdam, 1978).

⁷P. Debye, *Polar Molecules* (Chemical Catalog, New York, 1929)

⁸K. S. Cole and R. H. Cole, J. Chem. Phys. 9, 341 (1941).

⁹S. Häsel, A. Poglitsch, L. Genzel, and F. Kremer, Biopolymers 25, 677 (1986).

¹⁰L. Genzel, F. Kremer, A. Poglitsch, and G. Bechtold, Biopolymers 22, 1715 (1983).

¹¹A. Poglitsch, F. Kremer, and L. Genzel, J. Mol. Biol. 173, 137 (1984).

¹²D. Weber, E. J. Zehnder (to be published).